Journal of Nuclear Medicine, published on August 1, 2013 as doi:10.2967/jnumed.112.115824

Stratification of ^{18}F-Labeled PET Imaging Agents for the Assessment of Antiangiogenic Therapy Responses in Tumors

Julian L. Goggi*[1,2], Romain Bejot*[1], Shehzahdi S. Moonshi[1], and Kishore K. Bhakoo[1]

[1]*Singapore Bioimaging Consortium (A*STAR), Helios, Singapore; and* [2]*Department of Physiology, Yong Loo Lin School of Medicine, National University of Singapore, Singapore.*

Successful antiangiogenic therapies have been developed for the treatment of various cancers, but not all patients respond. Therefore, the early determination of therapy efficacy is essential for patient management. This study was done to evaluate the utility of various PET imaging biomarkers for early determination of the response to therapy with the antiangiogenic agent axitinib, a multiple receptor tyrosine kinase inhibitor, in tumors with diverse biologic characteristics. **Methods:** Mice bearing U87-MG and MDA-MB-231 subcutaneous tumors were treated with axitinib (25 mg/kg intraperitoneally daily for 10 d), and tumor volumes were assessed with caliper measurements. The animals were concurrently imaged longitudinally with ^{18}F-FDG, 3′-deoxy-3′-^{18}F-fluorothymidine (^{18}F-FLT), and 2-^{18}F-fluoroethyl-triazolyl conjugated c(RGDyK) peptide (^{18}F-FtRGD) to determine the optimal radiopharmaceutical for measuring the early treatment response in the 2 tumor types. **Results:** Daily administration of axitinib successfully retarded the growth of both U87-MG and MDA-MB-231 subcutaneous tumors, with significant differences in tumor volumes being observed from day 7 after therapy on. ^{18}F-FDG revealed a treatment efficacy response only at day 10 after treatment in both U87-MG tumor–bearing and MDA-MB-231 tumor–bearing animals. ^{18}F-FLT afforded earlier detection of the therapy response, revealing a significant difference between drug- and vehicle-treated animals at day 3 for animals bearing U87-MG tumors and at day 7 for animals bearing the more slowly growing MDA-MB-231 tumors. ^{18}F-FtRGD showed a rapid change in tumor retention that reached significance by day 7 in U87-MG tumor–bearing animals; in contrast, no significant difference in tumor retention was observed in MDA-MB-231 tumor–bearing animals. **Conclusion:** Longitudinal imaging with different radiopharmaceuticals displays various characteristics in different tumor types, depending on their biologic characteristics. Such studies may provide clinically important information to guide patient management and monitor the response to antiangiogenic therapy with the optimum noninvasive imaging agent in the relevant cancer type.

Key Words: angiogenesis; tumor; RGD; ^{18}F-FDG; ^{18}F-FLT

J Nucl Med 2013; 54:1–7
DOI: 10.2967/jnumed.112.115824

Angiogenesis, the formation of new blood vessels, is a hallmark of cancer progression and is essential for the development of solid tumors (*1*). In recent years, research has focused on the development of antiangiogenic therapies for the treatment of various cancers, including gliomas, breast cancers, and lung carcinomas (*2,3*). Successful therapies include the targeted antibody bevacizumab (Avastin; Genentech) and the receptor tyrosine kinase inhibitors sunitinib (Sutent; Pfizer) and axitinib (Inlyta; Pfizer). Although these therapies have largely been successful, some patients do not respond (*4–6*). Therefore, early determination of therapy efficacy is of benefit for patient management.

Molecular imaging for the determination of therapy efficacy in tumors is now relatively common in clinical practice, and many new molecular imaging agents are being developed to improve the application of noninvasive molecular imaging in oncology (*7*). At present, ^{18}F-FDG PET imaging is used routinely to assess the efficacy of cancer treatments. The glucose analog ^{18}F-FDG provides a surrogate measure of glucose metabolism in the tumor and surrounding tissue accumulating in proportion to its metabolism (*8*). However, the utility of ^{18}F-FDG for the assessment of therapy can be complicated by high ^{18}F-FDG uptake in surrounding tissue or other benign pathologies; therefore, low-grade or small tumors may exhibit little differential ^{18}F-FDG uptake (*9,10*).

Radiolabeled nucleosides have also been investigated as PET imaging agents for the assessment of therapy responses in tumors, with the benefit that they may also help provide information about histologic grade (*11*). 3′-Deoxy-3′-^{18}F-fluorothymidine (^{18}F-FLT) correlates with thymidine kinase 1 activity expressed during the DNA synthesis phase of the cell cycle, thus providing information on the proliferative potential of the tumor tissue (*12,13*). However, ^{18}F-FLT has proven to be an ineffective measure of therapy responses in some tumor types treated with antiangiogenic agents (*14*).

More recently, new molecular imaging agents that target key molecular biomarkers for the angiogenic cascade—namely, the integrins $\alpha_v\beta_3$, $\alpha_v\beta_5$, and $\alpha_5\beta_1$—have been developed (*15*). These integrins act as receptors for proteins expressing the arginine-glycine-aspartate (RGD) tripeptide sequence (*16,17*). Molecular imaging agents based on this RGD tripeptide sequence have been developed in a bid to improve the detection of both tumors and early therapeutic responses (*18,19*).

In this study, we compared the utility of the molecular imaging agents ^{18}F-FDG, ^{18}F-FLT, and 2-^{18}F-fluoroethyl-triazolyl conjugated c(RGDyK) peptide (^{18}F-FtRGD) for assessment of the early response to therapy with the multiple receptor tyrosine kinase inhibitor axitinib in rodent models of breast cancer and glioma. Our goal was to determine whether differences in tumor

Received Oct. 17, 2012; revision accepted Mar. 18, 2013.
For correspondence or reprints contact: Julian L. Goggi, Singapore Bioimaging Consortium (A*STAR), Helios, 07-10, 11 Biopolis Way, 138667 Singapore.
E-mail: julian_goggi@sbic.a-star.edu.sg
*Contributed equally to this work.
Published online ■■■■.

biology can affect patient management and the choice of an agent for the noninvasive monitoring of antiangiogenic treatment efficacy.

MATERIALS AND METHODS

Radiochemistry

All chemicals obtained commercially were of analytic grade and were used without further purification. Solvents and chemicals were purchased from Sigma-Aldrich unless stated otherwise. Reference compound ^{18}F-FLT was purchased from ABX. ^{18}F-FDG was purchased from Singapore Radiopharmaceuticals.

No-carrier-added ^{18}F-fluoride was produced by the $^{18}O(p,n)^{18}F$ nuclear reaction with a 16-MeV proton beam generated by a PETtrace cyclotron (GE Healthcare) in a silver target with ^{18}O-H_2O (Singapore Radiopharmaceuticals). A TracerLab FX_{FN} radiochemistry module (GE Healthcare) equipped with an S-1122 pump (Sykam) and a K-2001 single-wavelength UV detector (Knauer) was used for radiopharmaceutical synthesis and semipreparative high-performance liquid chromatography (HPLC) purification.

Radioactive analytic HPLC was performed with a PerkinElmer series 200 HPLC system equipped with a single-wavelength UV detector and a Flow-Ram NaI/PMT radiodetector (LabLogic). Thin-layer chromatography was performed on silica gel thin-layer chromatography plates (Sigma-Aldrich) and analyzed with an EZ-Scan radio-TLC strip scanner (Carroll & Ramsey). Levels of residual solvents were analyzed by use of a Varian 430 gas chromatograph with a flame ionization detector and a Varian Factour-Four VF-200 mass spectrometry column (30 m, 0.32 mm, 1 μm).

^{18}F-FLT and ^{18}F-FtRGD were produced by nucleophilic fluorination on the basis of previously described procedures (*19,20*). ^{18}F-FLT was produced with a high radiochemical purity (>99%) and a specific activity of 150–270 GBq/μmol and was formulated in isotonic saline solution (pH 6.5–7.5), with a radioactive concentration of 1.0–2.0 GBq/mL at the end of synthesis. ^{18}F-FtRGD was produced with a high radiochemical purity (>98%) and a specific activity of 10–50 GBq/μmol and was formulated in isotonic phosphate-buffered saline solution (pH 6.5–7.5), with a radioactive concentration of 0.5–6.0 GBq/mL at the end of synthesis.

Animals

All animal experiments were performed in accordance with Institutional Animal Care and Use Committee (IACUC) guidelines under IACUC 090437. A total of 70 outbred female nude CD1 mice were purchased from the Biological Resources Centre and housed at constant temperature (23°C) and humidity (40%) with a regular light–dark cycle.

Cancer Cells

Human U87-MG glioma cancer and MDA-MB-231 breast ductal carcinoma cells were purchased from the American Type Culture Collection. The cells were cultured in Dulbecco modified Eagle medium (Invitrogen) supplemented with 10% fetal bovine serum, penicillin (100 U/mL), and streptomycin (100 μg/mL) at 37°C in a humidified atmosphere with 5% CO_2. The cells were subsequently trypsinized and washed 3 times in Dulbecco modified Eagle medium. A cell suspension was then mixed with an equal volume of Matrigel (BD Biosciences) to provide a cell concentration of 3×10^7 cells/mL. Mildly anesthetized animals (under isoflurane) were injected subcutaneously in the right shoulder with 3×10^6 cells in a volume of 0.1 mL within 60 min of the final dissociation and counting processes. In all 36 animals receiving implanted breast tumors, 17β-estradiol pellets (0.72 mg, 60-d sustained release) were implanted subcutaneously with a trocar (Innovative Research of America) 24 h before tumor injection.

Dosing Regimen

At 3–5 wk after injection of tumor cells, the mice were divided into 2 treatment groups. One group received daily administrations of axitinib (Selleck Pharmaceuticals) at a dose of 25 mg/kg by intraperitoneal injection, and the other group received intraperitoneal administrations of the vehicle alone (polyethylene glycol–H_2O, 30:70) as previously described (*21*). Axitinib was well tolerated; no significant effects on animal health were observed.

Tumor Volume Studies

Throughout the study, the sizes of the tumors were measured with calipers. The volume of a tumor was calculated with the equation $[a \times (b \times b)]/0.523$, where a is the longest measurement and b is the shortest measurement.

In Vivo Imaging Studies

The animals from the axitinib-treated cohort and from the vehicle-treated cohort were randomly assigned to groups to be imaged with one of the imaging agents (^{18}F-FDG, ^{18}F-FLT, or ^{18}F-FtRGD). Small-animal PET and CT imaging with ^{18}F-FDG, ^{18}F-FLT, or ^{18}F-FtRGD was performed on days 0, 1, 3, 7, and 10 after initiation of the dosing regimen.

Each group of animals was injected in the lateral tail vein with a solution of ^{18}F-FDG, ^{18}F-FLT, or ^{18}F-FtRGD. The animals were imaged under isoflurane anesthesia (2% alveolar concentration), and biologic monitoring for respiration and temperature was performed with a BioVet system (m2m imaging). Small-animal PET imaging was performed with a Siemens Inveon PET/CT scanner (Siemens Inc.).

Animals in the ^{18}F-FDG group ($n = 7$ for U87-MG and $n = 4$ for MDA-MB-231) were kept fasting for 12 h before injection with ~3 MBq per animal and were imaged statically at 40–60 min after injection. Animals in the ^{18}F-FLT group ($n = 7$ for U87-MG and $n = 4$ for MDA-MB-231) were injected with ~5 MBq per animal and were imaged statically at 30–50 min after injection. Animals in the ^{18}F-FtRGD group ($n = 4$ for U87-MG and $n = 7$ for MDA-MB-231) were injected with ~10 MBq per animal and were imaged statically at 70–90 min after injection.

Low-dose CT images (40 kV, 500 μA, 4 × 4 binning, 200-μm resolution) were acquired for anatomic registration and attenuation correction. Images were reconstructed with the image reconstruction, visualization, and analysis programs supplied by the manufacturer, and PET and CT data were analyzed with Amide software (Sourceforge 10.3; http://amide.sourceforge.net).

The uptake of radioactivity in a tumor was determined by placement of a volume of interest around the tumor delineated on the CT images. A volume of interest was also placed around a region of the muscle in the lower left hind limb to provide reference tissue values. The tissue concentrations were determined with volume-of-interest analysis and are presented as percentage injected dose per gram (%ID/g).

Microvascular Density (MVD) Measurement

Once assayed for radioactivity on day 10, the tumors were immediately excised and fixed in neutral buffered formalin. The MVD of a tumor was quantified with a method previously described by Wedge et al. (*22*). Tumor specimens were fixed, stained for CD34 with a chromagen endpoint, and analyzed (without knowledge of treatment assignment) with a KS400 instrument (Imaging Associates). The MVD was calculated as the number of CD34-positive vessels in 5,000 μm^2 of viable tumor area in each tumor section.

Tumor Proliferation Assay

After the MVD was determined, the Ki67 staining of a tumor was quantified with a method previously described by Viel et al. *(23)*.

jnm115824-pe ■ 7/26/13

Tumor specimens were treated with proteinase K at room temperature for 5 min and 5% serum blocking solution for 10 min, incubated overnight at 4°C with antihuman Ki67 monoclonal antibody diluted 1:75 (Dako), and visualized with a secondary antibody and 3,3′-diaminobenzidine tetrahydrochloride staining. Slides were analyzed (without knowledge of treatment) with a Leica SCN400 slide scanner (Leica Microsystems) and the "Measure Stained Cells" algorithms of Slidepath Tissue IA software (Leica Microsystems). Scanning and image analysis were performed at the Advanced Molecular Pathology Laboratory, Institute of Molecular and Cell Biology, Singapore.

RESULTS

Effect of Axitinib on U87-MG and MDA-MB-231 Tumor Sizes

Figures 1A and 1B show the average changes in tumor volumes (mean ± SD) from tumor inoculation, from treatment baseline (day 0, before axitinib or vehicle administration), and on each of the imaging days. From (and including) day 3 after initiation of the dosing regimen, there was a discernible difference in tumor diameter between the axitinib-dosed group and the vehicle-dosed group for both U87-MG tumor–bearing animals and MDA-MB-231 tumor–bearing animals; however, in both cases the difference did not reach significance until day 7 ($P < 0.01$ for U87-MG and $P < 0.05$ for MDA-MB-231; 2-tailed unpaired t test). Volume and diameter data were confirmed with CT measurements (data not shown). [Fig. 1]

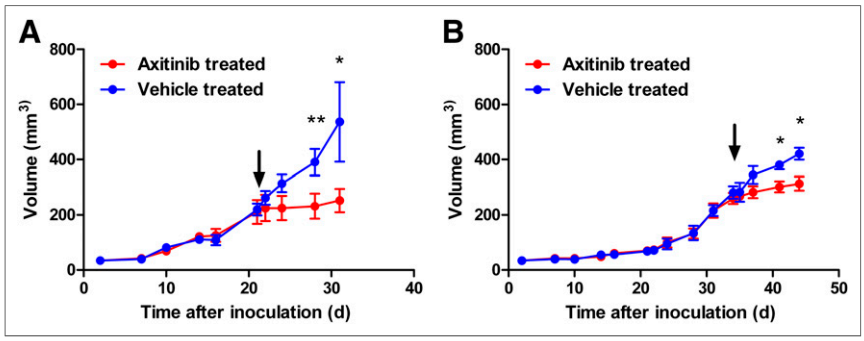

FIGURE 1. Growth kinetics of U87-MG tumors (A) and MDA-MB-231 tumors (B) in vehicle-treated animals and axitinib-treated animals (volume is reported in mm^3 [mean ± SD; $n = 4$]). Arrows denote day 0, 1 d before initiation of therapy regimen. $^*P < 0.05$. $^{**}P < 0.01$.

Effect of Axitinib on U87-MG and MDA-MB-231 Tumor Uptake of ^{18}F-FDG

The U87-MG tumor uptake of ^{18}F-FDG (Table 1) was significantly reduced only in the axitinib-treated group, not in the vehicle-treated group, at day 10 after treatment initiation ($P < 0.01$; 2-tailed unpaired t test comparing normalized data). [Table 1] Figure 2A shows the data normalized to day 0. Overall, the uptake of ^{18}F-FDG was lower in MDA-MB-231 tumors than in U87-MG tumors. Tumor uptake in the vehicle-treated animals was relatively stable from day 0 on (Table 1). Treatment with axitinib induced a slight reduction in ^{18}F-FDG uptake that only reached significance by day 10 after therapy initiation (day 0) ($P < 0.01$; 2-tailed t test comparing normalized data). Figure 2B shows the data normalized to day 0. [Fig. 2]

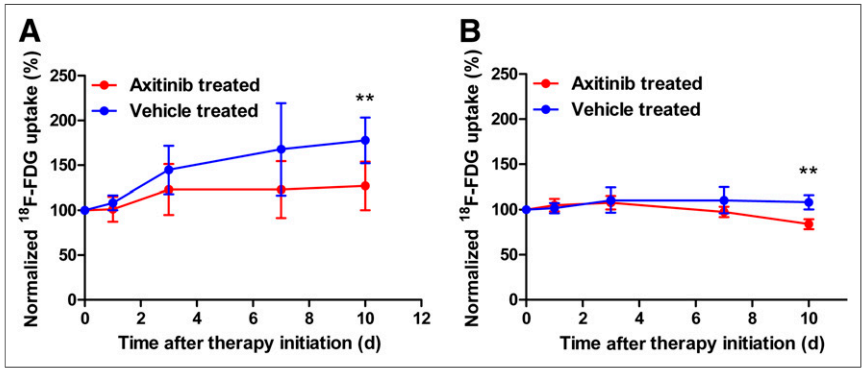

FIGURE 2. Uptake of ^{18}F-FDG in U87-MG tumors (A; $n = 7$) and MDA-MB-231 tumors (B; $n = 4$) in vehicle-treated animals and axitinib-treated animals, normalized to day 0 (% normalized uptake from day 0 [mean ± SD]). $^{**}P < 0.01$.

Effect of Axitinib on U87-MG and MDA-MB-231 Tumor Uptake of ^{18}F-FLT

Axitinib induced a significant therapy response, as measured by ^{18}F-FLT, in U87-MG tumors by day 3 after treatment initiation ($P < 0.05$ at day 3, $P < 0.01$ at day 7, and $P < 0.05$ at day 10; 2-tailed t test comparing normalized data). The vehicle-treated group showed increasing tumor uptake of ^{18}F-FLT from day 0 on, whereas in the axitinib-treated group tumor uptake remained stable (Table 2). Figure 3A shows the data normalized to day 0. The data showed that the uptake of ^{18}F-FLT was lower in MDA-MB-231 tumors than in U87-MG tumors. Tumor uptake in the vehicle-treated animals stayed steady during the 10 d after treatment initiation. Treatment with axitinib [Table 2] [Fig. 3]

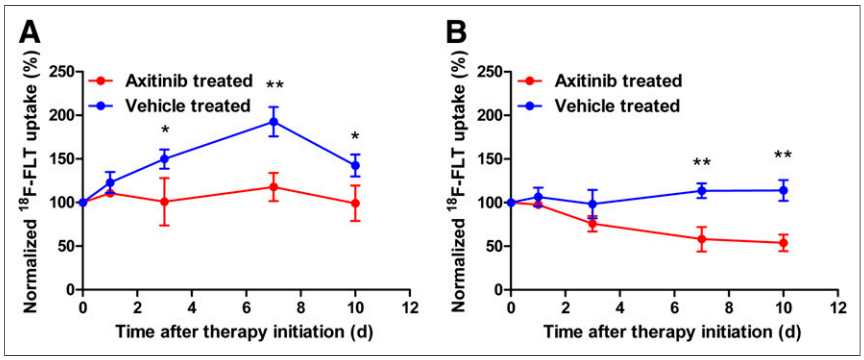

FIGURE 3. Uptake of ^{18}F-FLT in U87-MG tumors (A; $n = 7$) and MDA-MB-231 tumors (B; $n = 4$) in vehicle-treated animals and axitinib-treated animals, normalized to day 0 (% normalized uptake from day 0 [mean ± SD]). $^*P < 0.05$. $^{**}P < 0.01$.

jnm115824-pe ■ 7/26/13

induced a reduction in tumor uptake of ^{18}F-FLT (Table 2) that reached significance by day 7 after therapy initiation ($P < 0.01$ at day 7 and $P < 0.01$ at day 10; 2-tailed t test comparing normalized data). Figure 3B shows the data normalized to day 0.

Effect of Axitinib on U87-MG and MDA-MB-231 Tumor Retention of ^{18}F-FtRGD

U87-MG tumor retention of ^{18}F-FtRGD was attenuated by axitinib therapy by day 7 after treatment initiation ($P < 0.05$ at day 7 and $P < 0.01$ at day 10; 2-tailed t test comparing normalized data). Tumor retention in the vehicle-treated animals increased steadily from day 0 on (Table 3). However, axitinib therapy stabilized tumor retention of ^{18}F-FtRGD. Figure 4A shows the data normalized to day 0. ^{18}F-FtRGD retention in MDA-MB-231 tumors was not significantly altered by the addition of axitinib over the time course studied (Table 3). In both vehicle- and axitinib-treated tumors, retention remained stable throughout the study. Figure 4B shows the data normalized to day 0.

[Table 3] [Fig. 4]

MVD Analysis

MVD, a marker of angiogenesis, was significantly lower in tumors from axitinib-treated mice than in tumors from vehicle-treated mice 10 d after therapy initiation (Fig. 5) for both U87-MG tumor–bearing mice ($P < 0.01$; $n = 10$) and MDA-MB-231 tumor–bearing mice ($P < 0.05$; $n = 10$). This significant reduction in MVD in axitinib-treated mice confirmed the therapeutic response of the tumors to axitinib. Figure 6 shows staining for endothelial cells with CD34 of representative tumor sections taken 10 d after the administration of axitinib or vehicle.

[Fig. 5] [Fig. 6]

The levels of Ki67, a marker of cell proliferation, were significantly lower in tumors from axitinib-treated mice than in tumors from vehicle-treated mice 10 d after therapy initiation (Fig. 7) for both U87-MG tumor–bearing mice ($P < 0.01$; $n = 6$) and MDA-MB-231 tumor–bearing mice ($P < 0.05$; $n = 6$). This significant reduction in Ki67 staining in axitinib-treated mice confirmed the therapeutic response of the tumors to axitinib.

[Fig. 7]

TABLE 1
Uptake of ^{18}F-FDG in U87-MG ($n = 7$) and MDA-MB-231 ($n = 4$) Tumors

	Uptake (mean ± SD %ID/g) of ^{18}F-FDG in:			
	U87-MG tumors		MDA-MB-231 tumors	
Days after treatment	Axitinib treated	Vehicle treated	Axitinib treated	Vehicle treated
0	3.03 ± 0.46	2.99 ± 0.31	1.84 ± 0.10	2.05 ± 0.16
1	3.07 ± 0.62	3.24 ± 0.33	1.93 ± 0.19	2.09 ± 0.17
3	3.76 ± 1.10	4.29 ± 0.60	1.98 ± 0.12	2.25 ± 0.19
7	3.66 ± 0.83	4.94 ± 1.20	1.79 ± 0.05	2.25 ± 0.20
10	3.68 ± 0.41	5.26 ± 0.48	1.54 ± 0.07	2.22 ± 0.21

TABLE 2
Uptake of ^{18}F-FLT in U87-MG ($n = 7$) and MDA-MB-231 ($n = 4$) Tumors

	Uptake (mean ± SD %ID/g) of ^{18}F-FLT in:			
	U87-MG tumors		MDA-MB-231 tumors	
Days after treatment	Axitinib treated	Vehicle treated	Axitinib treated	Vehicle treated
0	3.02 ± 1.18	2.82 ± 0.69	3.37 ± 0.33	2.90 ± 0.46
1	3.47 ± 1.23	4.3 ± 0.14	3.28 ± 0.29	3.08 ± 0.53
3	3.37 ± 0.84	4.9 ± 0.68	2.54 ± 0.24	2.89 ± 0.83
7	2.65 ± 0.60	4.14 ± 0.56	1.99 ± 0.68	3.29 ± 0.53
10	3.34 ± 0.60	4.68 ± 0.89	1.84 ± 0.50	3.30 ± 0.55

TABLE 3
Uptake of ^{18}F-FtRGD in U87-MG ($n = 4$) and MDA-MB-231 ($n = 7$) Tumors

	Uptake (mean ± SD %ID/g) of ^{18}F-FtRGD in:			
	U87-MG tumors		MDA-MB-231 tumors	
Days after treatment	Axitinib treated	Vehicle treated	Axitinib treated	Vehicle treated
0	1.62 ± 0.32	1.50 ± 0.25	1.59 ± 0.72	1.58 ± 0.41
1	1.66 ± 0.23	1.74 ± 0.29	1.69 ± 0.17	1.71 ± 0.14
3	1.37 ± 0.29	1.61 ± 0.43	1.07 ± 0.28	1.36 ± 0.06
7	1.43 ± 0.22	2.40 ± 0.56	2.01 ± 0.54	1.90 ± 0.59
10	1.65 ± 0.25	3.33 ± 0.63	1.28 ± 0.06	1.50 ± 0.03

jnm115824-pe ■ 7/26/13

RGB

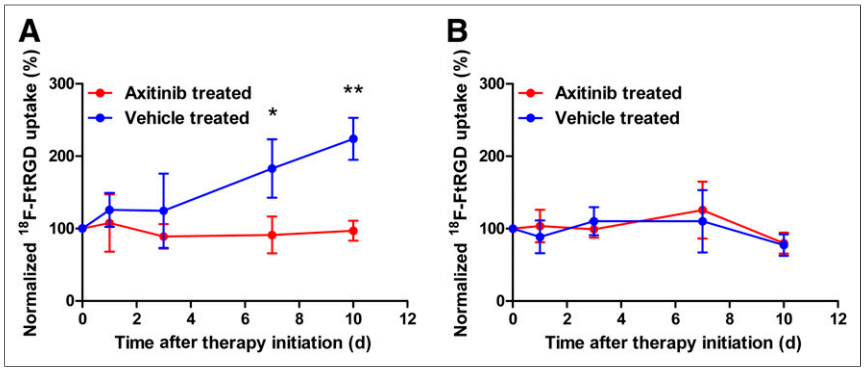

FIGURE 4. Uptake of ^{18}F-FtRGD in U87-MG tumors (A; $n = 4$) and MDA-MB-231 tumors (B; $n = 7$) in vehicle-treated animals and axitinib-treated animals, normalized to day 0 (% normalized uptake from day 0 [mean ± SD]). $^{*}P < 0.05$. $^{**}P < 0.01$.

RGB

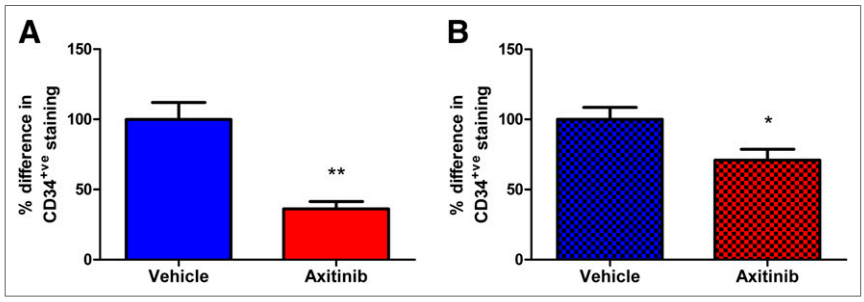

FIGURE 5. Angiogenesis (represented by MVD) in U87-MG and MDA-MB-231 tumors. MVD was significantly lower in both U87-MG tumors (A; $n = 10$) and MDA-MB-231 tumors (B; $n = 10$) from axitinib-treated mice than in tumors from vehicle-treated mice 10 d after treatment initiation. Data are reported as percentage difference in CD34-positive (CD34^{+ve}) staining per square millimeter, normalized to average for vehicle-treated specimens. $^{*}P < 0.05$. $^{**}P < 0.01$.

RGB

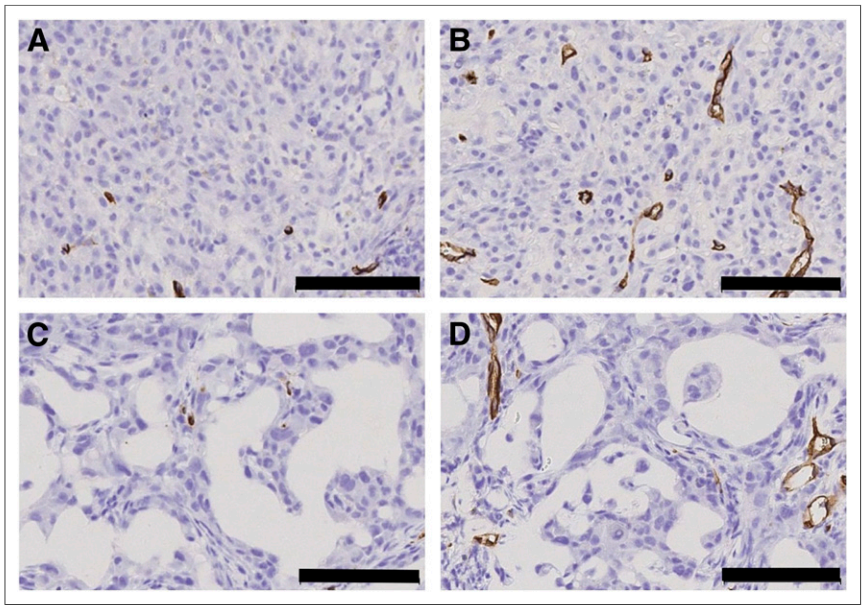

FIGURE 6. Representative sections were taken from both tumor types 10 d after initiation of therapy regimen. Representative sections from axitinib-treated U87-MG tumors (A) and MDA-MB-231 tumors (C) were analyzed for MVD after staining for endothelial cells with CD34 (bars = 100 μm) and compared with sections from vehicle-treated U87-MG tumors (B) and MDA-MB-231 tumors (D).

DISCUSSION

Various methods are used clinically to assess antiangiogenic therapies in tumors; these methods include measuring blood flow and blood volume (dynamic contrast-enhanced CT and MR imaging), which assess the downstream effects of angiogenesis (*24–26*). However, PET imaging has the ability to directly measure processes in the angiogenesis pathway and potentially provide a more specific means to assess antiangiogenic therapy efficacy in tumors. Much of the utility of radiopharmaceuticals is dependent on the biology of tumors and their biochemical environment. The 2 cell lines chosen for evaluation in this study were U87-MG, a human glioma that grows rapidly and induces significant vascular changes, and MDA-MB-231, a human ductal breast carcinoma that grows slowly and induces little vascular modification (*27*).

^{18}F-FDG was able to detect treatment responses in both tumor types; however, a statistical difference in tumor uptake was not observed until day 10 after therapy initiation, demonstrating that ^{18}F-FDG is a relatively insensitive measure of a therapy response. The ability of ^{18}F-FDG to diagnose tumors in vivo is well documented, but multiple studies have shown the limitations (such as the complication of uptake in benign nonpathologic tissue and inflammation) of ^{18}F-FDG in the determination of a therapy response (*28–30*).

In contrast, ^{18}F-FLT, which acts as a surrogate measure of tumor cell proliferation, revealed significant treatment responses by 3 d in the more rapidly growing glioma tumor and 7 d in the more slowly growing breast cancer. This improvement in early therapy determination through the use of ^{18}F-FLT may be attributable to vascular effects, which may be more prominent in U87-MG tumors. However, the Ki67 data indicated similar levels of inhibition of the proliferation rate by the axitinib treatment in the 2 tumor types. Therefore, the higher basal proliferation rate and the higher ^{18}F-FLT baseline uptake observed in U87-MG tumors may have made therapy efficacy easier to detect (*31*).

As expected from previous reports on integrin-binding ligands (*18*), ^{18}F-FtRGD showed an excellent ability to detect a therapy response in the U87-MG model by day 7. Interestingly, this radiopharmaceutical revealed no therapy response in the MDA-MB-231 breast cancer model, despite

jnm115824-pe ■ 7/26/13

RGB

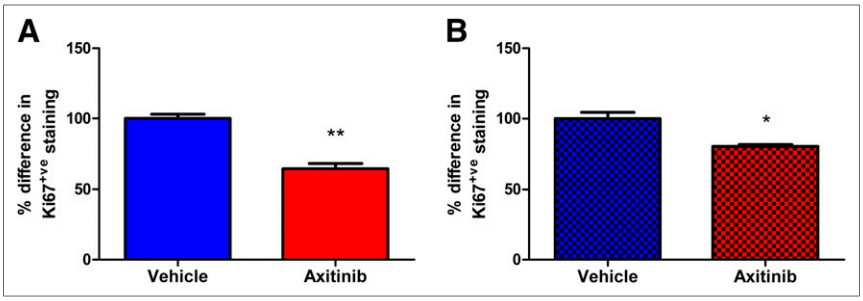

FIGURE 7. Rate of proliferation (Ki67) of U87-MG and MDA-MB-231 tumors. Ki67 levels were significantly lower in both U87-MG tumors (A; $n = 6$) and MDA-MB-231 tumors (B; $n = 6$) from axitinib-treated mice than in tumors from vehicle-treated mice 10 d after treatment initiation. Data are reported as percentage difference in Ki67-positive ($Ki67^{+ve}$) cells per square millimeter, normalized to average for vehicle-treated specimens. $^{*}P < 0.05$. $^{**}P < 0.01$.

a significant suppression of tumor growth observable in the tumor volume.

The uptake of RGD-containing radiopharmaceuticals has been shown to be well correlated with the expression of integrin $\alpha_v\beta_3$ and with the density of $\alpha_v\beta_3$-expressing microvessels (*32,33*). The 2 tumor cell lines chosen for this study had different levels of expression and localization of $\alpha_v\beta_3$. U87-MG tumors have been shown to express high levels of $\alpha_v\beta_3$ on both the vasculature and the cell surface (*32,34,35*), whereas MDA-MB-231 tumors have a very low level of cell surface expression of $\alpha_v\beta_3$: the integrin is found essentially only on the vasculature (*36*). The inability of ^{18}F-FtRGD to monitor a therapy response in MDA-MB-231 tumors may have been related to the low levels of $\alpha_v\beta_3$ expressed on the tumor cells themselves. Indeed, an early therapy response to the tyrosine kinase inhibitor ZD4190 has been shown in the ductal breast carcinoma MDA-MB-435, which has a high level of expression of $\alpha_v\beta_3$ on the cell surface (*36,37*). However, previous studies indicated that RGD-containing ligands are capable of measuring therapy responses in other rapidly growing tumor types that have a low level of cell surface expression of $\alpha_v\beta_3$, such as the Lewis lung carcinoma model (*38*). Therefore, it is likely that multiple biologic factors, including the lower level of vascularization and slow growth rate of MDA-MB-231 tumors, coupled with the reduced number of available cell surface binding sites, affect the sensitivity of RGD radiopharmaceutical binding and the ability to measure a therapy response in this tumor type.

CONCLUSION

The radiopharmaceuticals evaluated in this study report on different aspects of tumor biology: glucose metabolism (^{18}F-FDG); thymidine kinase activity and, hence, proliferation (^{18}F-FLT); and angiogenesis (^{18}F-FtRGD). The ability of each of these radiopharmaceuticals to measure therapy efficacy after treatment with the antiangiogenic agent axitinib appears to be dependent on the characteristics of the tumors to be evaluated. These data suggest that differences in tumor biology may be critical for individual patient management and the choice of radiopharmaceutical agents for the noninvasive monitoring of therapy efficacy.

DISCLOSURE

The costs of publication of this article were defrayed in part by the payment of page charges. Therefore, and solely to indicate this fact, this article is hereby marked "advertisement" in accordance with 18 USC section 1734. The authors would like to acknowledge the kind support of BMRC, A*STAR, for funding this research. No other potential conflict of interest relevant to this article was reported.

REFERENCES

1. Carmeliet P, Jain RK. Angiogenesis in cancer and other diseases. *Nature.* 2000;407:249–257.
2. de Boüard S, Herlin P, Christensen JG, et al. Antiangiogenic and anti-invasive effects of sunitinib on experimental human glioblastoma. *Neuro Oncol.* 2007;9:412–423.
3. Fratto ME, Imperatori M, Vincenzi B, Tomao F, Santini D, Tonini G. New perspectives: role of sunitinib in breast cancer. *Clin Ter.* 2011;162:251–257.
4. Dawson SJ, Conus NM, Toner GC, et al. Sustained clinical responses to tyrosine kinase inhibitor sunitinib in thyroid carcinoma. *Anticancer Drugs.* 2008;19:547–552.
5. Scott BJ, Quant EC, McNamara MB, Ryg PA, Batchelor TT, Wen PY. Bevacizumab salvage therapy following progression in high-grade glioma patients treated with VEGF receptor tyrosine kinase inhibitors. *Neuro Oncol.* 2010;12:603–607.
6. Yuasa T, Takahashi S, Hatake K, Yonese J, Fukui I. Biomarkers to predict response to sunitinib therapy and prognosis in metastatic renal cell cancer. *Cancer Sci.* 2011;102:1949–1957.
7. Vallabhajosula S. ^{18}F-labeled positron emission tomographic radiopharmaceuticals in oncology: an overview of radiochemistry and mechanisms of tumor localization. *Semin Nucl Med.* 2007;37:400–419.
8. Kubota R, Kubota K, Yamada S, Tada M, Ido T, Tamahashi N. Active and passive mechanisms of [fluorine-18] fluorodeoxyglucose uptake by proliferating and prenecrotic cancer cells in vivo: a microautoradiographic study. *J Nucl Med.* 1994;35:1067–1075.
9. van der Hiel B, Pauwels EK, Stokkel MP. Positron emission tomography with 2-[^{18}F]-fluoro-2-deoxy-D-glucose in oncology, part IIIa: therapy response monitoring in breast cancer, lymphoma and gliomas. *J Cancer Res Clin Oncol.* 2001;127:269–277.
10. Price SJ. Advances in imaging low-grade gliomas. *Adv Tech Stand Neurosurg.* 2010;35:1–34.
11. Saga T, Kawashima H, Araki N, et al. Evaluation of primary brain tumors with FLT-PET: usefulness and limitations. *Clin Nucl Med.* 2006;31:774–780.
12. Francis DL, Freeman A, Visvikis D, et al. In vivo imaging of cellular proliferation in colorectal cancer using positron emission tomography. *Gut.* 2003;52:1602–1606.
13. Price SJ, Fryer TD, Cleij MC, et al. Imaging regional variation of cellular proliferation in gliomas using 3′-deoxy-3′-[^{18}F]fluorothymidine positron-emission tomography: an image-guided biopsy study. *Clin Radiol.* 2009;64:52–63.
14. Honer M, Ebenhan T, Allegrini PR, et al. Anti-angiogenic/vascular effects of the mTOR inhibitor everolimus are not detectable by FDG/FLT-PET. *Transl Oncol.* 2010;3:264–275.
15. Beer AJ, Kessler H, Wester HJ, Schwaiger M. PET imaging of integrin alphaV-beta3 expression. *Theranostics.* 2011;1:48–57.
16. Giancotti FG, Ruoslahti E. Integrin signaling. *Science.* 1999;285:1028–1032.
17. Horton MA. The alpha v beta 3 integrin "vitronectin receptor." *Int J Biochem Cell Biol.* 1997;29:721–725.
18. Battle MR, Goggi JL, Allen L, Barnett J, Morrison MS. Monitoring tumor response to antiangiogenic sunitinib therapy with ^{18}F-fluciclatide, an ^{18}F-labeled $\alpha_V\beta_3$-integrin and $\alpha_V\beta_5$-integrin imaging agent. *J Nucl Med.* 2011;52:424–430.
19. Bejot R, Goggi J, Moonshi SS, Robins EG. A practical synthesis of [^{18}F]FtRGD: an angiogenesis biomarker for PET. *J Labelled Comp Radiopharm.* In press.
20. Kim DW, Ahn DS, Oh YH, et al. A new class of SN2 reactions catalyzed by protic solvents: facile fluorination for isotopic labeling of diagnostic molecules. *J Am Chem Soc.* 2006;128:16394–16397.
21. Wilmes LJ, Pallavicini MG, Fleming LM, et al. AG-013736, a novel inhibitor of VEGF receptor tyrosine kinases, inhibits breast cancer growth and decreases vascular permeability as detected by dynamic contrast-enhanced magnetic resonance imaging. *Magn Reson Imaging.* 2007;25:319–327.
22. Wedge SR, Kendrew J, Hennequin LF, et al. AZD2171: a highly potent, orally bioavailable, vascular endothelial growth factor receptor-2 tyrosine kinase inhibitor for the treatment of cancer. *Cancer Res.* 2005;65:4389–4400.

23. Viel T, Talasila KM, Monfared P, et al. Analysis of the growth dynamics of angiogenesis-dependent and -independent experimental glioblastomas by multimodal small-animal PET and MR imaging. *J Nucl Med.* 2012;53:1135–1145.
24. Navis AC, Hamans BC, Claes A, et al. Effects of targeting the VEGF and PDGF pathways in diffuse orthotopic glioma models. *J Pathol.* 2011;223:626–634.
25. Kharuzhyk SA, Petrovskaya NA, Vosmitel MA. Diffusion-weighted magnetic resonance imaging in non-invasive monitoring of antiangiogenic therapy in experimental tumor model. *Exp Oncol.* 2010;32:104–106.
26. Wu X, Jeong EK, Emerson L, Hoffman J, Parker DL, Lu ZR. Noninvasive evaluation of antiangiogenic effect in a mouse tumor model by DCE-MR imaging with Gd-DTPA cystamine copolymers. *Mol Pharm.* 2010;7:41–48.
27. Doblas S, He T, Saunders D, et al. Glioma morphology and tumor-induced vascular alterations revealed in seven rodent glioma models by in vivo magnetic resonance imaging and angiography. *J Magn Reson Imaging.* 2010;32:267–275.
28. Abouzied MM, Crawford ES, Nabi HA. ^{18}F-FDG imaging: pitfalls and artifacts. *J Nucl Med Technol.* 2005;33:145–155.
29. van Waarde A, Cobben DC, Suurmeijer AJ, et al. Selectivity of ^{18}F-FLT and ^{18}F-FDG for differentiating tumor from inflammation in a rodent model. *J Nucl Med.* 2004;45:695–700.
30. Lee TS, Ahn SH, Moon BS, et al. Comparison of ^{18}F-FDG, ^{18}F-FET and ^{18}F-FLT for differentiation between tumor and inflammation in rats. *Nucl Med Biol.* 2009;36:681–686.
31. Zhang CC, Yan Z, Li W, et al. [^{18}F]FLT-PET imaging does not always "light up" proliferating tumor cells. *Clin Cancer Res.* 2012;18:1303–1312.
32. Beer AJ, Haubner R, Sarbia M, et al. Positron emission tomography using [^{18}F] galacto-RGD identifies the level of integrin alpha(v)beta3 expression in man. *Clin Cancer Res.* 2006;12:3942–3949.
33. Haubner R, Weber WA, Beer AJ, et al. Noninvasive visualization of the activated alphavbeta3 integrin in cancer patients by positron emission tomography and [^{18}F]galacto-RGD. *PLoS Med.* 2005;2:e70.
34. Takano S, Kamiyama H, Tsuboi K, Matsumura A. Angiogenesis and antiangiogenic therapy for malignant gliomas. *Brain Tumor Pathol.* 2004;21:69–73.
35. Takano S, Tsuboi K, Tomono Y, Mitsui Y, Nose T. Tissue factor, osteopontin, alphavbeta3 integrin expression in microvasculature of gliomas associated with vascular endothelial growth factor expression. *Br J Cancer.* 2000;82:1967–1973.
36. Taherian A, Li X, Liu Y, Haas TA. Differences in integrin expression and signaling within human breast cancer cells. *BMC Cancer.* 2011;11:293–308.
37. Yang M, Gao H, Yan Y, et al. PET imaging of early response to the tyrosine kinase inhibitor ZD4190. *Eur J Nucl Med Mol Imaging.* 2011;38:1237–1247.
38. Morrison MS, Ricketts SA, Barnett J, Cuthbertson A, Tessier J, Wedge SR. Use of a novel Arg-Gly-Asp radioligand, ^{18}F-AH111585, to determine changes in tumor vascularity after antitumor therapy. *J Nucl Med.* 2009;50:116–122.

jnm115824-pe ■ 7/26/13